International Journal of Offshore and Polar Engineering (ISSN 1053-5381)
Copyright © by The International Society of Offshore and Polar Engineers
Vol. 22, No. 3, September 2012, pp. 193–199

http://www.isope.org/publications

A Semi-Infinite Numerical Wave Flume using Smoothed Particle Hydrodynamics

E. Didier
LNEC (Laboratório Nacional de Engenharia Civil) - NPE, Lisboa, Portugal
MARETEC (Marine and Environmental Technology Center), Instituto Superior Técnico
Universidade Técnica de Lisboa, Lisboa, Portugal

M. G. Neves
LNEC (Laboratório Nacional de Engenharia Civil) - NPE, Lisboa, Portugal

This paper presents the new boundary condition implemented in the LNEC SPH numerical model based on the SPHysics model and on a standard Smoothed Particle Hydrodynamic formulation: the piston-type wave maker includes now dynamic wave absorption and allows simulating a semi-infinite flume. Verification of the active wave maker absorption is carried out through the simulation of the interaction between a regular incident wave and an impermeable vertical breakwater. Results show that the active wave-maker allows outgoing waves to be absorbed and reflection at the wave-maker to be avoided.

INTRODUCTION

Numerical modeling of the interaction among waves and coastal structures is a challenge due to the many nonlinear phenomena involved, such as, wave propagation, wave transformation with water depth, interaction among incident and reflected waves, run-up / run-down and wave overtopping.

Numerical models, more or less complex depending on the approach and on the physical assumptions, allow simulating the propagation of waves and the near shore transformation. The models based on the nonlinear Boussinesq equations, such as COULWAVE (Lynett and Liu, 2004), give good predictions comparing with field data and laboratory physical modeling. However, it does not model the breaking and highly nonlinear processes that occur when waves impinge the coastal structures, such as overtopping. Numerical models based on Euler or Navier-Stokes equations, such as CANAL (Clément, 1996), based on Boundary Element Method, or FLUINCO (Teixeira, 2001), based on a mixed Euler-Lagrange formulation of the free surface, allow modeling wave-structure interaction and calculating velocity and pressure field. However, those numerical models do not simulate wave breaking.

Only few numerical models allow simulating the very complex phenomena of wave breaking and overtopping. Those models are generally based on fluid dynamic equations, i.e. the Navier-stokes equations, and developed using an Eulerian approach. Numerical simulation of free surface flows is treated using the Volume of Fluid (VOF) approach (Hirt and Nichols, 1981), such as the Reynolds Average Navier-Stokes (RANS) model COBRAS-UC (Lara et al., 2006). However, the accuracy o[1]f wave breaking and overtopping simulations strongly depend on the mesh and a fine grid is necessary to ensure modeling those phenomena.

Recently, models based on Lagrangian methods, such as the Smoothed Particle Hydrodynamics (SPH) approach, have emerged. The method is based on the Navier-Stokes equations and a completely mesh-free technique. Monaghan (1994) shows the first application of Lagrangian method for modeling free surface flows. The recent advances on Smoothed Particle Hydrodynamics models, since 1994, show that Lagrangian method is a very promising alternative approach to simulate wave breaking and overtopping due to its completely mesh-free technique. Several numerical models are constructed using the SPH method. One of these is the SPHysics model (Crespo, 2008; Crespo et al., 2008a, 2008b), inspired by the formulation of Monaghan (1992).

The SPH numerical model used and developed at the LNEC (National Laboratory of Civil Engineering) is based on the original SPHysics model and specially developed for studies of wave interacting with impermeable and porous structures. This model aims to be a useful tool for real case studies of coastal engineering. Promising agreement with experimental data has been obtained for both free surface elevation and overtopping discharge for impermeable coastal structures (Didier and Neves, 2009a, 2009b, 2010a, 2010b; Didier et al., 2011). The present numerical model includes two specific developments: i) a partial renormalization (i.e. partial filtering density), where renormalization is applied only for particles near the structure, which is an original method that allows simultaneously propagating waves, without diffusion, and modeling accurately the pressure field near the structure (Didier et al., 2011); ii) an active wave maker absorption that allows to simulate a semi-infinite numerical wave flume.

This paper presents the implementation of the active wave maker absorption in the SPH numerical model and an application to wave interacting with an impermeable vertical breakwater that allows verifying the dynamic absorption technique.

SET OF EQUATIONS

The bi-dimensional momentum conservation equation in a continuum field and the conservation law, in Lagrangian form, for a viscous fluid are written as

$$\frac{dv}{dt} = -\frac{1}{\rho}\nabla P + \Pi + g \tag{1}$$

$$\frac{1}{\rho}\frac{d\rho}{dt} = -\text{div}\ (v) \tag{2}$$

Received October 15, 2011; revised manuscript received by the editors February 13, 2012. The original version was submitted directly to the Journal.
KEY WORDS: Smoothed Particle Hydrodynamics (SPH), wave dynamic absorption, coastal engineering.

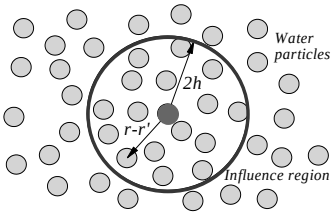

Fig. 1 Compact support of the kernel

where v refers to the velocity, P the pressure, ρ the fluid density, Π the diffusion terms and g=(0, -9.81m/s^2) the gravitational acceleration.

SPH APPROACH

The partial differential equations of continuum fluid dynamics (Eqs. 1 and 2) are transformed into SPH forms, i.e. particle forms, by integral equations using integral interpolants (Monaghan, 1992; Gingold and Monaghan, 1977; Liu, 2003). The fundamental principle is to approximate any function $A(r)$ by:

$$A(r) = \int_\Omega A(r')W(r-r',h)dr' \tag{3}$$

where r is the vector position, W is the weighting function, h is called the smoothing length. The interpolation function, i.e. weighting function or kernel, allows determining the interaction among neighboring particles included in the influence domain, controlled by the smoothing length h, typically higher than the initial particle spacing. Fig. 1 shows a typical compact support of a kernel function. Numerically, the kernel is a function with compact support within a region determined by a radius of 2h. The kernels should be verified several conditions of positivity, compact support, Delta function behavior. Different kernels were developed and can be found in the literature (Liu, 2003).

The relation given in Eq. 3 is written as an approximation of the function A at a particle a, in discrete notation:

$$A(r) = \sum_b m_b \frac{A_b}{\rho_b} W_{ab} \tag{4}$$

where the summation is over all the particles within the region of compact support of the kernel function. The mass and density are noted m_b and ρ_b respectively and W_{ab}=$W(r_a$-$r_b, h)$ is the kernel.

Two types of SPH model were developed: strict incompressible and weakly incompressible SPH model. The major differences between the weakly compressible SPH (Monaghan, 1992; Dalrymple et al., 2001) and the incompressible SPH (Gotoh et al., 2001, 2004; Shao and Lo, 2003; Shao, 2010) lie in that the former calculated the pressures explicitly using an equation of state, while the latter employs a strict incompressible formulation for what the pressure is obtained implicitly by solving a pressure Poisson equation derived from the mass and momentum equations.

SPH NUMERICAL MODEL

The actual SPH model used and developed at the LNEC is based on the SPHysics code, an open-source Smoothed Particle Hydrodynamics program developed jointly by researchers of several Universities (Crespo, 2008; Crespo et al., 2008a, 2008b; Gómez-Gesteira et al., 2008, 2010) and includes mainly two specific developments: i) a partial renormalization (i.e. partial filtering density) (Didier et al., 2011); ii) an active wave maker absorption that allows to simulate a semi-infinite numerical wave flume.

The fluid in the standard SPH formalism is treated as weakly compressible. The numerical model presents a modular form and a variety of features are available, such as 2D and 3D models, various kernels and viscosity models (artificial, laminar and Sub-Particle Scale turbulence model), density filter (Shepard or MLS), and solid boundary conditions (dynamic boundaries, repulsive forces). Detail of numerical implementation is available in (Gómez-Gesteira et al., 2008; SPHysics code v1.4, 2008). The actual LNEC's version of SPH model is especially devoted to studies of hydrodynamics around maritime structures and allows analyzing the phenomena involved in wave-structure interaction, including free surface elevation, wave overtopping, velocity profiles, pressure and forces on the structure.

For numerical simulations of wave propagation, the quadratic kernel (Johnson et al., 1996; Dalrymple and Rogers, 2006) is used to determine the interaction between the particles. This kernel has the particularity of not having an inflection point in its first and second derivative in the range of function definition.

$$W(q,h) = \frac{3}{2\pi h^2}\left(\frac{q^2}{4} - q + 1\right) \quad \text{for} \quad 0 \le q \le 2 \tag{5}$$

where q=(r_a-r_b)/h.

In the present computational method, the fluid is treated as weakly compressible which allows the use of an equation of state to determine fluid pressure. The relationship between the pressure and the density was assumed to follow the equation of state provided by Batchelor (1974) (see latter).

In the SPH equations, the discrete equation of conservation of momentum is given by

$$\frac{Dv_a}{Dt} = \sum_b m_b \left(\frac{P_a}{\rho_a^2} + \frac{P_b}{\rho_b^2} + \Pi_{ab}\right).\nabla_a W_{ab} + g \tag{6}$$

where t is the time, g=(0, 0, -9.81)m.s^{-2} is the gravity acceleration, v_a, P_a and ρ_a are the velocity, the pressure and the density of a particle a, respectively, P_b, ρ_b and m_b are the pressure, the density and the mass of a particle b included in the influence region of the kernel, W_{ab} is the kernel and Π_{ab} the viscosity term. Finaly, $\nabla_a W_{ab}$ is given by:

$$\nabla_a W_{ab} = \nabla_a W(r_a - r_b) = \frac{\partial W_{ab}}{\partial x_a} i + \frac{\partial W_{ab}}{\partial y_a} j \tag{7}$$

where i and j are the unit vectors in the direction of the coordinate axis and (x_a, y_a) are the coordinates of particle a.

In SPHysics, three models for the viscous terms Π_{ab} are implemented: the artificial viscosity model (Monaghan, 1992), the laminar viscosity model (Morris et al., 1997) and the laminar viscosity turbulence SPS – Sub-Particle Scale (Gotoh et al., 2001; Rogers and Dalrymple, 2004). The latter model is used in the present simulations because it includes not only a model of laminar viscosity but also the effects related to the turbulence through a model derived from the LES-type models (Large Eddy Simulation). It was shown, in previous study (Didier and Neves, 2009b), that Sub-Particle Scale turbulence model provided better results compared to artificial viscosity model since SPS model avoids the strong dissipative effects of artificial viscosity model (the wave amplitude decreases as the parameter of the model of artificial viscosity increases). Consequently the SPS turbulence model is used in the present simulations.

The equation of mass conservation in the discrete SPH formalism is given by:

$$\frac{d\rho_a}{dt} = \sum_b m_b (u_a - u_b).\nabla_a W_{ab} \tag{8}$$

The particles move according to the following equation:

$$\frac{dr_a}{dt} = u_a + \varepsilon \sum_b m_b \frac{v_{ab}}{\bar{\rho}_{ab}} W_{ab} \tag{9}$$

where v_{ab}=v_a-v_b and $\bar{\rho}_{ab}$=(ρ_a-ρ_b)/2. The last term of the equation, including the parameter ε, corresponds to the correction term XSPH of Monaghan (1989). Particles are usually moved using the XSPH Monaghan formulation, with ε=0.5 (values ranged between 0 and 1). The method is a correction for the particle velocity, which is recalculated taking into account the velocity of that particle and the average velocity of neighbouring particles. However, it was shown in Didier and Neves (2009b) that instabilities appear during wave propagation due to the XSPH correction, particles cross the solid boundary, fluid flow exhibits unphysical behaviors and the program crashes. Consequently, in the present simulations, the XSPH correction is not used and ε=0.

The equation of state (Batchelor, 1974), which relates the pressure in the fluid with the density, is given by:

$$P = B\left[\left(\frac{\rho}{\rho_0}\right)^{\gamma} - 1\right] \tag{10}$$

where γ=7 and $B = c_0^2 \rho_0 / \gamma$, the reference density ρ_o=1000 kg/m^3 and c_o the sound velocity. With this approach, the compressibility is adjusted to slow the speed of sound so that the time step in the model, based on the sound velocity, is reasonable and CPU time is reduced.

Numerically, integration in time is performed by the Predictor-Corrector model using a variable time step.

The repulsive boundary condition, developed by Monaghan and Kos (1999), is used and allows preventing a water particle crossing a solid boundary. Finally, a variable time step is used to ensure the CFL condition.

Initially, the water particles are placed in the flume using a Cartesian distribution, i.e. particles are regularly distributed, with spacing between particles defined by *do*. This is a condition of SPH method when smoothing length of the kernel is constant. Velocity is zero and pressure is hydrostatic. Fig. 2 presents a view of the initial distribution of solid and fluid particles near a structure.

More details of numerical implementation of the SPH model can be found in the User's program SPHysics (Gómez-Gesteira et al., 2008) and in Gómez-Gesteira et al. (2010).

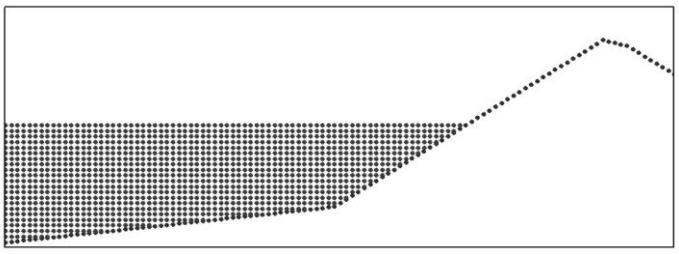

Fig. 2 Typical initial distribution of solid and fluid particles

While the kinematics of SPH simulations is generally realistic, the pressure field of the particles can exhibit large pressure oscillations. Gómez-Gesteira et al. (2010) shows that renormalization (filter density) is necessary to obtain a good representation of a dam-break flow and pressure field without oscillations. However, renormalization influence is more complex for wave propagation. One of the most straightforward and computationally least expensive methods to smooth out pressure oscillations is to perform a filter over the density of the particles and to re-assign a density to each particle (Colagrossi and Landrini, 2003). However, Didier et al. (2011) shown that total renormalization, i.e. renormalization on all fluid particles, stabilizes the pressure field but causes a numerical diffusion of wave propagation and a large reduction on wave height, incompatible with experimental results. On the other hand, without renormalization, unphysical pressure fluctuations occur and forces on structures cannot be calculated. Didier et al. (2011) show that partial renormalization, i.e. renormalization applied only for particles near the structure (at the end of the flume), seems to be a promising compromise and an original method that allows simultaneously propagating waves, without diffusion, and modeling accurately the pressure field near a structure or a beach.

WAVE GENERATION AND DYNAMIC ABSORPTION

Piston-type wave maker

In original SPHysics model (Gómez-Gesteira et al., 2008; SPHysics code v1.4, 2008), wave generation is performed moving the solid particles of the wave maker boundary, similar to the experimental flume. Waves are generated from the left to the right of the numerical flume. The wave maker movement is simulated in the model at any given time step, *t*, through the position $X_b(t)$ and velocity $U_b(t)$ of the solid particles constituting the wave maker. $X_b(t)$ and $U_b(t)$ are calculated using two equations, deduced from the linear wave theory and, for a regular wave, given by the following relations:

$$X_b(t) = X_b(t_o) + A_b \sin (2\pi t / T) \tag{11}$$

where T is the incident wave period, A_b the wave maker amplitude (depending of the wave height H), $X_b(t_o)$ the initial position of the wave maker and t the time. The velocity of the wave maker is calculated by the derivation of Eq. 11 in the time and is given by

$$U_b(t) = 2\pi A_b / T \cos (2\pi t / T) \tag{12}$$

It is necessary, in numerical applications, to smooth the velocity at the beginning of the movement to avoid numerical instabilities due to the impulsive starting of the wave maker movement. Smoothing is achieved here by using a small ramp, which corresponds to adding a *tanh* term in Eqs. 11 and 12.

Active wave maker absorption

Active wave maker absorption is included in the LNEC's SPH model, using the same procedure followed in physical flumes: the numerical wave maker is equipped with a control system for simultaneous wave generation and active wave absorption.

The methodology proposed by Shäffer and Klopman (2000) is followed. This procedure, based on the wave maker movement used in the experiments, was also implemented in a Reynolds Averaged Navier-Stokes type model using a Volume of Fluid technique for modeling free surface flow by Lara et al. (2011), with good results.

The target wave maker position, $X_b(t)$, is corrected in real time in order

to absorb outgoing waves and to avoid reflection at the wave maker. The position of the wave maker is obtained through the velocity corrections of the wave maker motion.

For that, it is necessary to estimate the free surface elevation of the reflected wave, η_R, to be absorbed, comparing the target-free surface, η_{target}, to the free surface recorded in front of the wave maker, η_{SPH}. The free surface elevation is measure at about 5*do* from the wave maker, with *do* being the initial distance between particles,

$$\eta_R = \eta_{target} - \eta_{SPH} \quad (13)$$

The wave maker velocity has to be modified in order to match the velocity induced by the wave to be absorbed. In this case, as wave generation is performed by piston-type wave maker, with uniform velocity over the water depth, wave absorption is made using linear long-wave theory (Shäffer and Klopman, 2000; Dean and Dalrymple, 1991),. So that, the velocity correction owing to absorption the reflected wave, U_R, can be written as follows:

$$U_R = \eta_R (g / h)^{1/2} \quad (14)$$

where g is the gravity acceleration and h is the water depth.

To obtain the desired wave maker position, velocity has to be integrated considering both the target velocity, U_{target}, calculated using Eq. 12 and the velocity correction for absorption, U_R,

$$X_b(t) = X_b(t_o) + \int_0^t \left(U_{target} + U_R\right) dt \quad (15)$$

Numerical implementation of the active wave maker absorption for the SPH model is described hereafter. Target wave maker velocity, U_{target}, at a time t is calculated by Eq. 12. As the wave maker is a piston-type, the velocity is the same for all solid particles of the wave maker.

The initial conditions, as for the case without dynamic absorption, are the wave maker with no velocity, $U_b(t_o)$=0.0, and at its initial position, $X_b(t_o)$.

Free surface elevation at the front of the wave maker is determined at a gauge located at 5*do* from the wave maker, as referred.

The target free surface elevation at time t is calculated using linear wave theory relation for a wave height H.

Velocity correction, U_R, is calculated using Eq. 14 and the value of free surface elevation of reflected wave, η_R, calculated by Eq. (13).

The corrected wave maker velocity, $U_b(t+dt)$, is obtained by the relation

$$U_b(t+dt) = U_{target} + U_R \quad (16)$$

Wave maker position at time $t+dt$, $X_b(t+dt)$, is deduced by extrapolation from the velocity at time $t+dt$ and t and by the previous position of the wave maker at time t, $X_b(t)$, using the following expression:

$$X_b(t+dt) = X_b(t) + (U_b(t+dt)+U_b(t))*dt / 2 \quad (17)$$

It was verified that the precision of the extrapolation using Eq. 17 is of order $O(6)$-$O(7)$, when comparing with the calculation of the wave maker position obtained by Eq. 11, from linear wave theory.

WAVE INTERACTING WITH A VERTICAL BREAKWATER

The case study presented here is wave interacting with an impermeable vertical breakwater. The breakwater is composed by a 0.181 m height berm, with a slope 1:3, and a vertical wall, located 0.2 m from the end of the slope, as shown in Figure 3. The crest freeboard is 0.3 m above the still water level. The horizontal bottom is 3.62 m length.

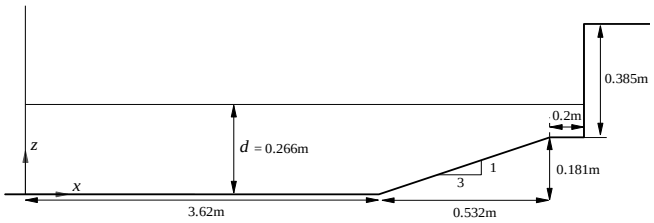

Fig. 3 Schematic representation of the semi-infinite wave flume and the structure, coordinate system and dimensions

The case study presented here is wave interacting with an impermeable vertical breakwater. The breakwater is composed by a 0.181 m height berm, with a slope 1:3, and a vertical wall, located 0.2 m from the end of the slope, as shown in Figure 3. The crest freeboard is 0.3 m above the still water level. The horizontal bottom is 3.62 m length.

Regular waves were tested with 1.3 s wave period, T, and 0.10 m wave height, H. Water depth, d, is 0.266 m, which result in a wave length, L, equal to 1.88 m.

Active absorption of the reflected waves at the wave maker was used in the present simulation.

A regular Cartesian grid is used for distributing the fluid particles into the computational domain, with a uniform distance, *do*, in horizontal and vertical directions equal to 3.97×10^{-3} m. The particle volume is equal to 1.576×10^{-5} m^3/m. The number of fluid and solid particles used for the present simulation is 69692 (1547 solid particles). Simulation is performed to 40 s which correspond to 31 waves. The mean time step is around 3.8×10^{-5} s.

Computational time in the present application of SPH code is around 92 hours for modeling 40 s, using a serial version of the code and a Personal Computer Intel(R) Core(TM) i7 CPU 930 @ 2.80GHz.

Verification of the accuracy of the active wave maker absorption is carried out analyzing the time series of the free surface elevation at x=2.0 and 2.5 m and of the forces on the vertical wall of the breakwater. Results are also compared with a case of a simple piston type wave maker without absorption to show the efficiency of the active wave maker absorption.

Figure 4 shows a comparison of the free surface elevation of the reflected wave, η_R, the target-free surface elevation, η_{target}, and the free surface elevation recorded in front of the wave maker, η_{SPH}. Numerically, a small velocity ramp is used at the beginning of the wave maker motion to avoid numerical instabilities near the wave maker. This explain the important differences showed between η_{target} and η_{SPH} until t =1.0 s. Before t=5.0 s, time when the reflected wave from the vertical wall reaches the wave maker, the reflected wave is around zero, the wave maker works only as a wave generator and the free surface elevation recorded in front of the wave maker is almost equal to the target one. At t=5.0 s, the active wave maker absorption starts to absorb the reflected waves.

For the present incident regular wave characteristics, the wave reflected by the breakwater is relatively regular, eventhough wave breaking occurs near the toe of the breakwater and the water column formed at the vertical wall after breaking induce a small randomness on the reflected amplitude.

For this case, the reflected wave amplitude, η_R, recorded in front of the wave maker is around 42% of incident wave amplitude. Reflection coefficient is also calculated using separation method of incident and reflected waves developed by Mansard and Funke (1980) and found to be equal to 47%, in accordance with the direct estimation of reflected wave amplitude in front of the wave maker.

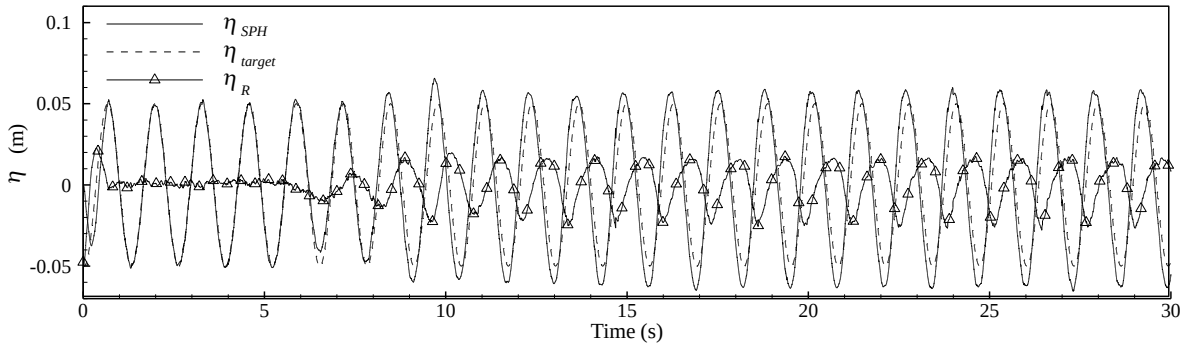

Fig. 4 Comparison of the free surface elevation of the reflected wave, η_R, the target-free surface, η_{target}, and the free surface recorded in front of the wave maker, η_{SPH}.

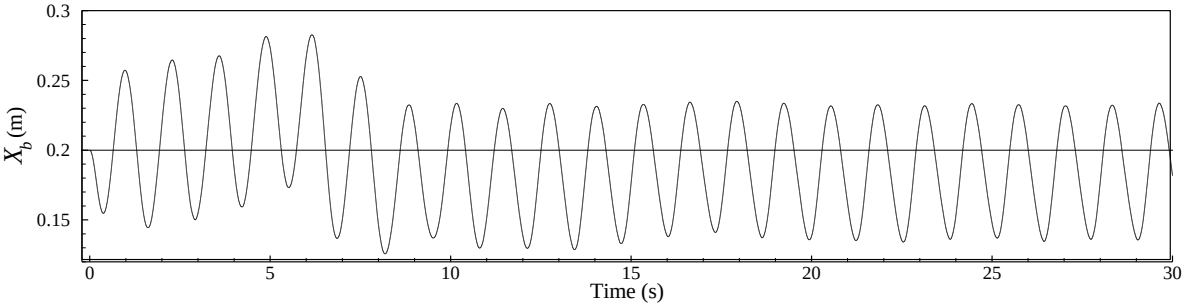

Fig. 5 Position of wave maker along the time (the horizontal solid line correspond to the initial position of wave maker).

For the present incident regular wave characteristics, the wave reflected by the breakwater is relatively regular, eventhough wave breaking occurs near the toe of the breakwater and the water column formed at the vertical wall after breaking induce a small randomness on the reflected amplitude.

For this case, the reflected wave amplitude, η_R, recorded in front of the wave maker is around 42% of incident wave amplitude. Reflection coefficient is also calculated using separation method of incident and reflected waves developed by Mansard and Funke (1980) and found to be equal to 47%, in accordance with the direct estimation of reflected wave amplitude in front of the wave maker.

All this behaviour shows that the wave absorption system is acting as expected, absorbing the reflection at the wave maker and generating the same incident wave along the time.

Figure 5 shows the time series of the wave maker position. The solid horizontal line indicates the initial position of the wave maker. From the beginning of the wave maker motion to t = 15.0 s, the wave maker position is strongly variable due to its adaptation to different wave configurations: first the incident wave only, incident and transitional reflected wave between t = 0s to t = 15 s and, finally, after t = 15 s, the incident and the regular reflected wave. After this time, as it can be observed in the Figure 5, the wave maker motion is very regular, reflecting the regular pattern of the reflected wave that is absorbed by it.

Although the oscillatory nature of the free surface elevation is simulated by an piston type movement, small deviations from zero, the expected mean free surface elevation at the front of wave maker, appear and will contribute to a slow drift of the paddle (Shäffer and Klopman, 2000). This effect can be observed in Figure 5, where the mean paddle position after some time of simulation does not correspond anymore to the initial wave maker position. However, in the present simulation, this small drift is not critical since the change in the mean value of the free surface elevation is only 0.001 m (i.e. 0.4% of the water depth). In order to prevent this effect in future applications, the paddle could be forced back to its zero position, technique classically used in laboratory facilities (Shäffer and Klopman, 2000).

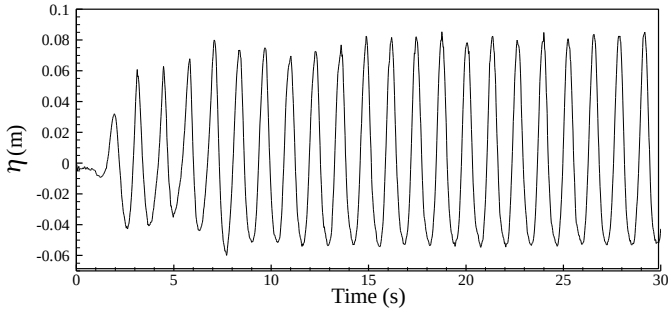

Fig. 6 Time series of free surface elevation at x=2.0 m

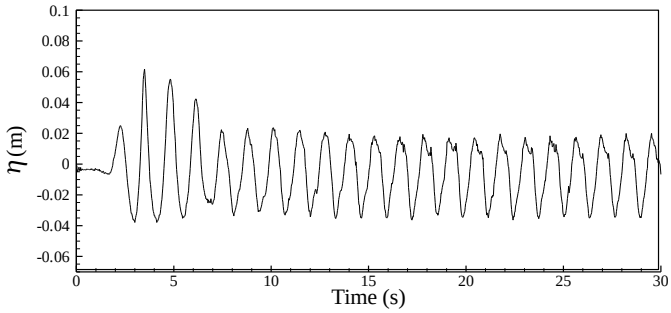

Fig. 7 Time series of free surface elevation at x=2.5 m

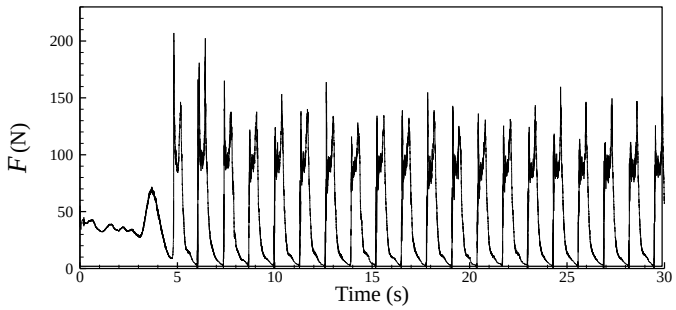

Fig. 8 Time series of force acting on the vertical wall of breakwater

Figure 6 and 7 present the time series of free surface elevation at x=2.0 and 2.5 m. The same pattern can be found at these gauges. Until t = 15.0 s, some variation of the free surface can be observed, due to the variation of the wave pattern, as explained before. After that, the wave form is more regular, even though, the mean position of the wave maker does not correspond to the initial position, due to the dynamic absorption. The differences on free surface elevation at these two gauges highlight the reflection phenomena. Comparing the free surface elevation at gauges x=2.0 m (Figure 6) and at x=2.5 m (Figure 7), it is possible to verify the influence of the reflected wave that increase free surface elevation at gauge x=2.0 m and decrease at gauge x=2.5 m, typical result of interaction between an incident and a reflected wave.

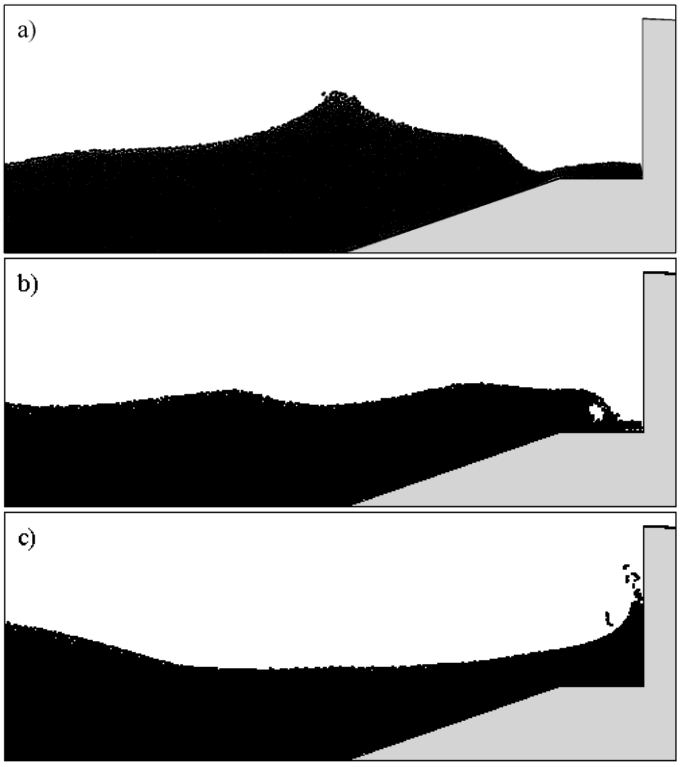

Fig. 9 Particle positions during the interaction between incident regular wave and vertical breakwater

The variation of the horizontal force on the frontal vertical wall of the breakwater is presented in Figure 8. In this signal, the effectiveness of

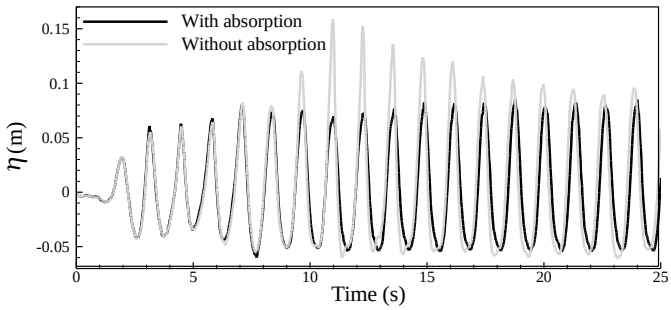

Fig. 10 Time series of free surface elevation at x=2.5 m with and without absorption

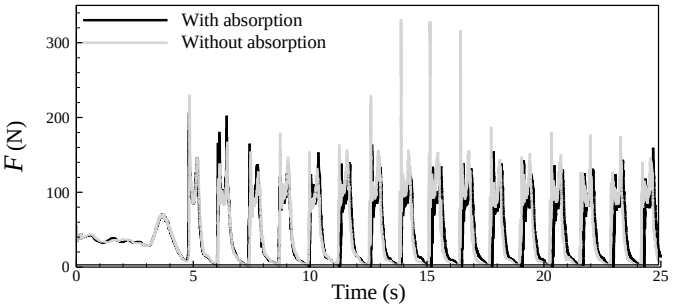

Fig. 11 Time series of force acting on the vertical wall of the breakwater with and without absorption

the wave maker absorption can be observed in the regularly of the signal along the time. Only small variability on the force can be observed, probably due to randomness of the wave breaking. The signal showed the expected pattern of the impact force, with two maxima the first corresponding to the wave impact on the vertical wall and the second to the collapse of the water column formed along the wall after the wave impact.

Figure 9 shows the fluid particle position near the vertical breakwater at time t=20.07 s, 20.33 s and 20.62 s. Figure 9a shows the strong interaction between the incident and the reflected wave that occurs near the structure. The increase of the free surface elevation is a result of the incident and reflected wave superposition. It can be seen that the water column is very small at the toe of the vertical wall. Figure 9b shows the wave attack on the structure. Reflected and incident wave are clearly identified in the figure. Wave breaks shortly before the vertical wall in a plunging breaking. After the wave impact on the toe of the wall, a water column appears along the vertical wall, Figure 9c, before collapse.

Figures 10 and 11 show a comparison of time series of free surface elevation at x=2.0 m and of force on the vertical wall of breakwater, respectively, obtained with the active wave maker absorption and with a simple type wave maker without absorption. Free surface elevation and force are strongly perturbed when absorption is not used due to the effect of successive wave reflection on the breakwater and on the paddle. Free surface elevation is largely increased, at this gauge, and force is strongly overestimated: without absorption, force reaches values about 320 N and decrease to values about 130 N when absorption is used. This very large difference is due to changes in the incident wave characteristic when active wave maker absorption is not used.

These comparisons allow verifying the effectiveness of active wave maker absorption, confirmed by the regularity of time series of free surface elevation and force when absorption is used. An analysis of

wave height variation at gauge x=2.0 m confirms also the efficiency of the active wave maker absorption: without absorption, the maximum difference of the wave height is about 0.023 m since with absorption the maximum difference is only 0.004 m.

CONCLUSIONS

Verification of the effectiveness of the active wave maker absorption, implemented in the LNEC´s version of SPH numerical model, based on the SPHysics model, is carried out through the simulation of the interaction between a regular incident wave and an impermeable vertical breakwater. Results show that active wave maker absorption allows to absorb outgoing waves and to avoid reflection at the wave maker. This new improvement on the model enable to enlarge the time calculation and to obtain large time series of free surface elevation, forces and pressure that allow correctly calculating statistics of overtopping, forces on the structures, etc.

Future works on the model include the validation of the active wave maker absorption for regular and irregular waves and the development of tools for modeling porous structures.

ACKNOWLEDGEMENTS

Eric Didier acknowledges the financial support given by the Portuguese Science and Technology Foundation, SFRH/BPD/37901/2007. The authors acknowledge the financial support given by the Portuguese Science and Technology Foundation for the Project SPACE - PTDC/ECM/114109/2009.

REFERENCES

Batchelor, GK (1974). "Introduction to Fluid Dynamics". Cambridge Univeristy Press, UK.

Clément, AH (1996). "Coupling of Two Absorbing Boundary Conditions for 2D Time-domain Simulations of Free Surface Gravity Waves", *J Comp Physics*, Vol 126, pp 139-151.

Colagrossi, A, and Landrini, M (2003), "Numerical simulation of interfacial flows by smoothed particle hydrodynamics", *J. Comp. Phys.*, Vol 191, pp 448–475.

Crespo, AJC (2008). "Application of the Smoothed Particle Hydrodynamics model SPHysics to free-surface hydrodynamics", Phd thesis, University of Vigo, Spain.

Crespo, AJC, Gómez-Gesteira, M, and Dalrymple, RA (2008a). "Modeling dam break behavior over a wet bed by a SPH technique", *Journal of Waterway, Port, Costal, and Ocean Engineering*, Vol 134(6), pp 313-320.

Crespo, AJC, Gómez-Gesteira, M, Narayanaswmy, MS, and Dalrymple, RA (2008b). "A hybrid Boussinesq-SPH model for coastal wave propagation", *Proc 3rd ERCOFTAC SPHERIC Workshop*, Lausanne, Switzerland, pp 11-16.

Dalrymple, RA, Knio, O, Cox, DT, Gomez-Gesteira, M, and Zou, S (2001). "Using Lagrangian particle method for deck overtopping", *Proc of the Waves ASCE*, pp 1082-1091.

Dalrymple, RA, and Rogers, BD (2006). "Numerical modeling of water waves with the SPH method", *Coastal Engineering*, Vol 53(2-3), pp 141-147.

Dean, RG, and Dalrymple, RA (1991). "Water wave mechanics for engineers and scientists", World Scientific, Singapore.

Didier, E, and Neves, MG (2009a). "Wave overtopping of a typical coastal structure of the Portuguese coast using a SPH model", *Journal of Coastal Research*, SI 56, pp 496-500.

Didier, E, and Neves, MG (2009b). "Coastal flow simulation using SPH: Wave overtopping on an impermeable coastal structure", *Proc 4th ERCOFTAC SPHERIC workshop*, pp 357-364, Nantes, France.

Didier, E, and Neves, MG (2010a). "A Lagrangian Smoothed Particles Hydrodynamics – SPH – method for modelling waves-coastal structure interaction", *Proc CFD2010 ECCOMAS*, Lisbon, Portugal.

Didier, E, and Neves, MG (2010b). "Study of wave interaction with coastal structures using a SPH numerical model", *Journal of Integrated Coastal Zone Management*.

Didier, E, Martins, R, Neves, MG, and Vasco, JRG (2011), "Interaction between wave and coastal structure: validation of two Lagrangian numerical models with experimental results", *Proc. MARINE 2011*, Lisbon.

Gómez-Gesteira, M., Rogers, BD, Dalrymple, RA, Crespo, AJC, and Narayanaswamy, M (2008). "User Guide for the SPHysics Code v1.4", http://wiki.manchester.ac.uk/sphysics.

Gómez-Gesteira, M, Rogers, BD, Dalrymple, RA, and Crespo, AJC (2010). "State-of-the-art of classical SPH for free-surface flows", *Journal of Hydraulic Research*, 48 Extra Issue, pp 6–27.

Gingold, RA, and Monaghan, JJ (1977). "Smoothed particle hydrodynamics: theory and application to non-spherical stars", *Monthly Notices of the Royal Astronomical Society*, Vol 181, pp 375-389.

Gotoh, H, Shibahara, T, and Sakai, T (2001). "Sub-particle-scale turbulence model for the MPS method – Lagrangian flow model for hydraulic engineering", *Computational Fluid Dynamics Journal*, Vol 9(4), pp 339-347.

Gotoh, H, Shao, SD, and Memita, T (2004). "SPH-LES model for numerical investigation of wave interaction with partially immersed breakwater", *Coastal Engineering Jpn*, Vol 46(1), pp 39-63.

Hirt, CW, and Nichols, BD (1981). "Volume of fluid VoF method for the dynamics of free boundaries", *J Comp Phys*, Vol 39, pp 201-225.

Johnson, G, Stryk, R, and Beissel, S (1996). "SPH for high velocity impact calculations", *Computer Methods in Applied Mechanics and Emgineering*, Vol 139, pp 347-373.

Lara, JL, Garcia, N, and Losada, IJ (2006). "RANS modelling applied to random wave interaction with submerged permeable structures", *Coastal Engineering*, Vol 53(5-6), pp 395-417.

Lara, JL, Ruju, A, and Losada, IJ (2011), "Reynolds averaged Navier-Stokes modelling of lon waves induced by transient wave group on a beach", *Proc. R. Soc. A*, Vol 467, pp 1215-1242.

Liu, GR (2003). "Mesh free methods. Moving beyond the finite element method". CRC press.

Lynett, P, and Liu, PL-F (2004). "Modelling wave generation, evolution and interaction with Depth-Integrated, Dispersive Wave equations", COULWAVE Code Manual. Cornell Univ. Long Inter. Wave Modelling Package.

Mansard, EPD, and Funke, ER (1980). "The Measurement of Incident and Reflected Spectra using Leat Squares Method", *Proc.17th Internation Conference on Coastal Engineering*, ASCE.

Monaghan, JJ (1989). "On the problem of penetration in particle methods", *Journal Computational Physics*, Vol 82, pp 1-15.

Monaghan, JJ (1992). "Smoothed Particle Hydrodynamics", *Annual Review of Astronomy and Astrophysics*, Vol 30, pp 543-574.

Monaghan, JJ (1994). "Simulating free surface flows with SPH", *Journal of Computational Physics*, Vol 110, pp 399-406.

Monaghan, JJ, and Kos, A (1999). "Solitary waves on a Cretan beach", *Journal of Waterways, Ports, Coastal and Ocean Engineering*, Vol 125, pp 145-154.

Morris, JP, Fox, PJ, and Zhu, Y (1997). "Modeling low Reynolds number incompressible flows using SPH", *Journal of Computational Physics*, Vol 136, pp 214-226.

Rogers, BD, and Dalrymple, RA (2004). "SPH modeling of breaking waves", *29th Int. Conference on Coastal Engineering*, World Scientific Press, pp 415-427.

Schäffer, H, and Klopman, G (2000), "Review of multidirectional active wave absorption methods", *J. Waterw. Port. Coast. Ocean Eng.*, Vol 126, pp 88–97.

Shao, SD, and Lo, EYM (2003). "Incompressible SPH method for simulating Newtonian and non-Newtonian flows with a free surface", *Adv Water Resour*, Vol 26(7), pp 787-800.

Shao, S (2010). "Incompressible SPH flow model for wave interactions with porous media", *Coastal Engineering*, Vol 57, pp 304-316.

SPHyscis code v1.4 (2008), http://wiki.manchester.ac.uk/sphysics

Teixeira, PRF (2001). "Simulação numérica da interacção de escoamentos tridimensionais de fluidos compressíveis e incompressíveis e estruturas deformáveis usando o método de elementos finitos", Phd thesis, PPGEC-UFRGS, Porto Alegre, Brasil.